Nonlinear inversion for earthquake rupture parameters

Peng Cheng Liu[(1)] and Ralph J. Archuleta[(2)]

(1) Institute for Crustal Studies, University of California, Santa Barbara, California, 93106, USA (e-mail: pcliu@crustal.ucsb.edu; phone; +1 805-893-4905). (2) Institute for Crustal Studies and Department of Geological Sciences, University of California, Santa Barbara, California, 93106, USA (e-mail: ralph@crustal.ucsb.edu; phone: +1 805-893-8441).

Abstract

The spatial distribution of rupture velocity, rise time, and intensity of high-frequency radiation on the fault strongly influence the ground motion. Because It is practically impossible to simulate deterministically high-frequency (frequency > 1.0 Hz) phase changes in ground acceleration, we invert the envelope of root-mean-square acceleration to determine these kinematic source parameters. The envelope inversion, a highly nonlinear problem, is solved by a hybrid global search algorithm. The synthetic acceleration waveforms are calculated by using empirical Green's functions. The Northridge earthquake inversions show the strongest radiation sources associated primarily with the beginning of the rupture (first 4 s) associated with the breaking of a high-stress-drop asperity. The rupture velocity is nearly uniform, about 3.0 km/s. The rise time is poorly resolved.

Introduction

The acceleration recordings from large earthquake contain abundant information of the dynamic rupture process on the fault. These recordings are generally dominated by amplitudes in the frequency range between 1.0-20 Hz. At these frequencies, it is practically impossible to reproduce the acceleration waveform analytically or numerically due to the small-scale complexity of source, path and site. Consequently, waveform inversions are not available in this frequency band. Waveform modeling has been successfully applied to determine the spatial distribution of earthquake fault rupturing process from strong motion records that are low passed at 2.0 Hz or less (e.g., Archuleta, 1984[1]; Hartzell and Heaton, 1983[2]; Wald *et al*., 1991[3]). Attempts have been made to extract information from strong motion recordings related to the high-frequency radiation process: Zeng *et al* .(1993)[4] used the envelope of the squared high-frequency (>5 Hz) displacement seismograms for inversion; Cocco and Boatwright (1993)[5] deconvolved the squared acceleration envelope; Kakehi and Irikura (1996[6], 1997[7]) and Hartzell *et al.*(1996)[8] inverted the envelope of root-mean-squared acceleration using small earthquake recordings as empirical Green's functions. If recordings of small earthquakes located within the rupture area

of large earthquake are available, they can be treated as empirical Green's functions (EGF) between source and site (Hartzell, 1978[9]). The major advantage of using EGFs in the inversion process is that it allows us to effectively separate seismic source parameters from the propagation effects (path and site) because these effects are included in EGFs.

The rupture velocity, rise time, and intensity of high-frequency radiation on the fault strongly affect the ground motion. Variations in these parameters are efficient sources of high frequency radiation (Madariaga, 1977[10],1983[11]; Das and Aki, 1977[12]). We parameterize the rupture process as the spatial distribution of high-frequency radiation intensity, rupture time and rise time on the fault. To solve for these parameters, we invert the acceleration envelopes using aftershock recordings as empirical Green's functions. The envelope inversion, a highly nonlinear problem, is solved using a search algorithm designed to find the global best solution of strong nonlinear problem (Liu *et al.*, 1995a,b[13, 14]).

We have applied this envelope inversion scheme to the 1994 Northridge earthquake. Because the acceleration envelopes contains no information about phase, we perform several tests to evaluate the applicability of envelope inversion and the effectiveness of using EGFs for determining the source parameters. We investigate the effects of source model parametrization on the inversions, the sensitivity of the source solutions to different EGFs, the effect of different windows lengths used to compute the envelope, and the dependence on the assumed fault geometry.

Method

The forward calculation of the ground motion time history is essential for analysis of rupture process on the fault. Theoretical calculations may lead to unreliable time histories, especially at high frequencies, because the crustal structure and local site effects are poorly known at the required wavelengths. An alternative approach, the empirical Green's function method (Hartzell, 1978[15]), is used to simulate the acceleration waveforms for the target event.

We divide the mainshock fault plane into subfaults, all with equal dimensions, and assume that the propagation effects from all subfaults to receiver can be represented by the record of a single, small event. We also assume that source spectra of subfault and aftershock obey the ω^{-2} scaling law (Aki, 1967[16]; Brune, 1970[17]). In frequency domain the seismogram from a large earthquake can be expressed as

$$A_l(f) = \sum_{j=1}^{N} W_j \frac{\frac{1}{\tau_s^2} + f^2}{\frac{1}{\tau_j^2} + f^2} A_s(f) \exp\left[-i\,2\pi f\,(t_{rj} + t_{sj})\right], \quad (1)$$

where $A_l(f)$ is spectrum of the synthetic accelerogram for the large earthquake; $A_s(f)$ is EGF accelerogram spectrum; N is the number of subfaults; R_j and τ_j are the hypocenter and rise time of subfault; R_s and τ_s are the hypocenter and rise time of small event; W_j is the weight factor reflecting the high-frequency radiation of subfault, i.e, it is the radiation intensity factor. For each subfault the seismogram is delayed by the S-wave travel time

from subfault to the receiver (t_{sj}) and by the time for the rupture to propagate from the hypocenter to the subfault (t_{rj}).

We invert for are the weighting factor, the rupture time and the rise time for each subfault. The radiation intensity W_j does not have an absolute value and may vary with different EGFs. Because of the difficulty of simulation of waveforms at high frequencies (>1 Hz), we use the acceleration envelope as inverse data (Kakehi and Irikura,1996[6], Hartzell, *et al*, 1996[8]). The envelope, $A_{rms}(t)$, is calculated by the running root mean square of the accelerogram, $a(t)$, in the time domain:

$$A_{rms}(t) = \sqrt{\frac{1}{2\Delta}\int_{t-\Delta}^{t+\Delta} a^2(t)\,dt}\,, \tag{2}$$

where, 2Δ is the smoothing window length.

We use the hybrid global search algorithm of Liu *et al*., 1995a,b[13, 14] to invert the data. The algorithm is based on a combination of simulated annealing with the downhill simplex method. This hybrid algorithm takes advantage the local search method, that performs well if the local model is suitable, and global methods that are can explore the full model space. Initially the random walk of the simulated annealing process dominates. As the temperature in the simulated is lowered, the simplex algorithm plays a more important role. The simulated annealing algorithm initially searches widely to find an appropriate model that is not far from the global minimum. Then the simplex algorithm moves the model quickly to the global minimum. Throughout the process the nonzero probability of large jumps allows the method to escape from local minima.

The hybrid global search method requires only the evaluation of objective function (misfit function), not its gradient. Following Sen and Stoffa (1991)[18], we define our objective function

$$obj = \sum_{1}^{N_p} W_p \left(1 - \frac{2\int D_p(t) S_p(t)\,dt}{\int D_p^2(t)\,dt + \int S_p^2(t)\,dt} \right), \tag{3}$$

In Eq (3) $D_p(t)$ is the data envelope, $S_p(t)$ is the corresponding synthetic envelope, and N_p is the number of records used in the inversion. W_p is the weight reflecting the quality of the data record, This objective function is a trade-off between least squares objective function and cross-correlation objective function.

Application to the 1994 Northridge earthquake

A large number of accelerographs recorded the January 17, 1994, Northridge earthquake (M_W=6.7) and its aftershock. Our envelope inversion requires mainshock and aftershock accelerograms recorded at the same site. The EGF accelerograms were recorded by portable stations. These sensors were collocated with strong-motion station by Southern California Earthquake Center (SCEC) and USGS. Two aftershocks (A, B) were used as the empirical Green's function events. Twelve stations recorded Event A and nine for event B. All three components of records are used. The acceleration time histories are bandpassed filtered from 1 to 20 Hz and uniformly sampled at a time step of 0.02s.

We assumed the same fault geometry as Wald *et al.* (1996): a fault with a strike of 122° and a dip of 40° to the southwest. The fault plane measures 20 km in length and extends from a depth of 5 km to 21 km for a downdip width of 24.9 km. The hypocenter is at

34.211° N, 118.546° W, depth of 17.5 km. The fault plane is discretized into 15× 15=225 subfaults. Each subfault has three model parameters: rupture time, rise time and weight factor. Because the simulated annealing part of the hybrid global search algorithm has a nonzero probability of making large jumps in the model, constraints are typically applied to the allowable values of the model parameters. The selection of these constraints is not crucial to the outcome of the inversion (assuming they do not exclude the global minimum), only to the amount of time required to reach the global minimum. We constrain the subfault rise time (τ_j) within the range of 0.1 to 5.0s. The rupture time (t_{rj}) of each subfault is bounded by the times for rupture to reach the subfault from the hypocenter, traveling at 2.0 and 4.0 km/s. The local rupture velocities may be less than 2.0 km/s or greater than 4.0 km/s, but the integrated velocity between the hypocenter and a given subfault is bounded between and 2.0 and 4.0 km/s. The weight factor (W_j) must be positive, but its upper bound depends on the magnitudes of mainshock and aftershock. Bounds of 0.0 and 40.0 are given for W_j (based on numerical test this is reasonable). In the inversion, the alignment of the data and synthetic records in time is accomplished by matching the synthetic S wave from the hypocenter with the first significant S wave arrival in the data.

Figure 1 shows the distribution of the high-frequency radiation intensities and the rupture times for the two separate inversions using the EGFs A and B. The left column is the fault solution obtained from aftershock A, the right is from aftershock B. At the top panel of Figure 1, we show our high-frequency radiation intensity inversion results. The details of the source locations of high-frequency radiation vary between the two inversions, but the general pattern is very consistent. The variation is probably due to the difference in depths, radiation patterns and travel path of the two aftershocks. The distribution of rupture time is nearly the same for both aftershocks. The distribution of the rise times differ significantly between these two inversions. The more uniform rise times are obtained for aftershock B. The inversion with different initial random distributions of source parameters produces similar results demonstrating that the envelope inversions are stable. The mechanism of the aftershock is not critical for the determination of the high-frequency radiation intensity and the rupture time; however, the rise times are sensitive to the choice of aftershock. It can also inferred that the distribution of the rise times have little influence on the high-frequency radiation intensity and the rupture time. To confirm this conclusion, we performed two other inversions similar except that the rise times were fixed at 2.0 s for all subfaults. The results agree closely with the distribution of weight factors and rupture times when the rise time was allowed to vary. This implies that while the high-frequency envelope inversion can not resolve the rise time, the lack of resolution has little effect on the high-frequency radiation intensity and the rupture time.

Results will be shown that provide other limitations and advantages of this method for inferring source parameters of finite faults.

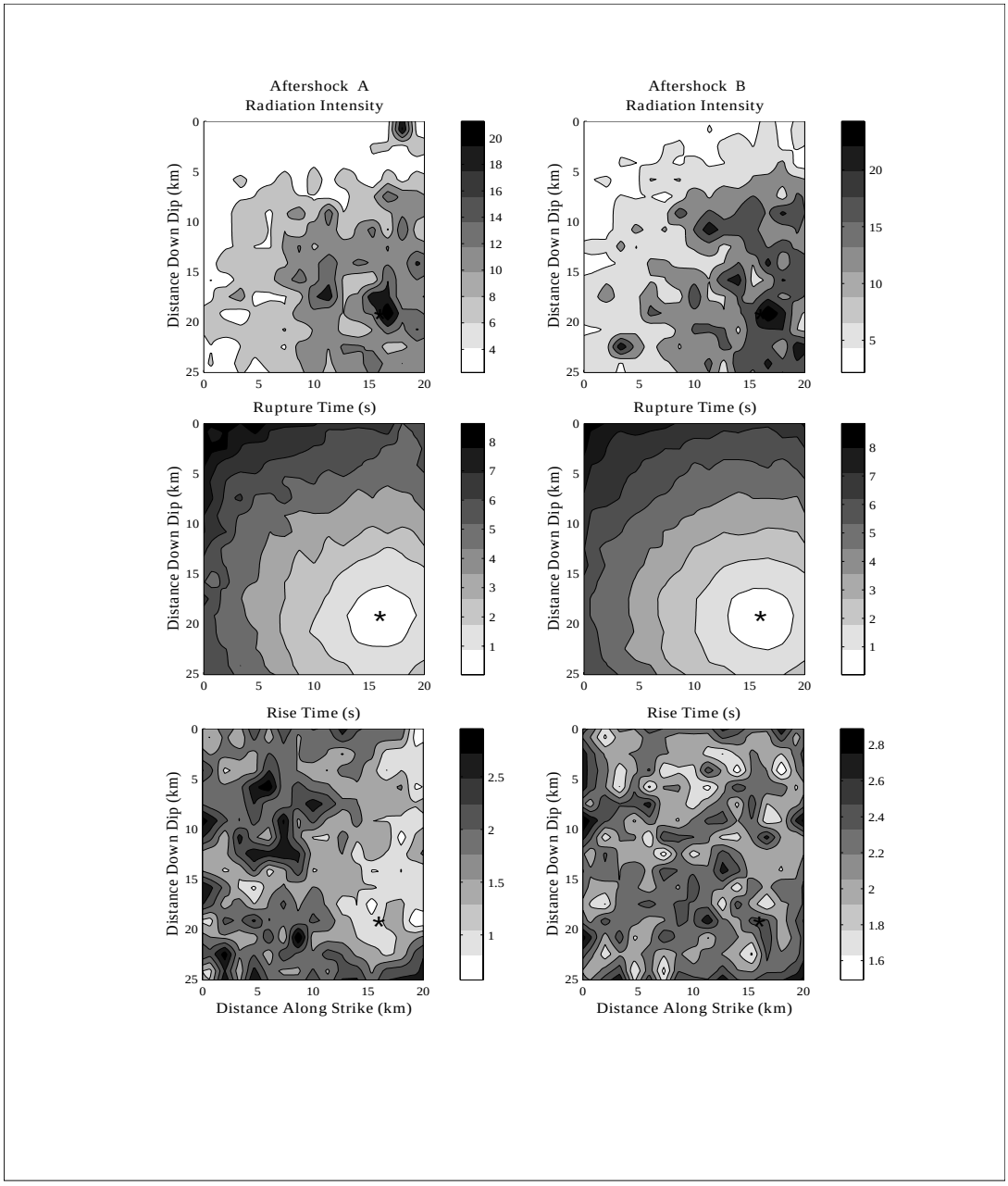

Figure 1: Spatial distribution of radiation intensity, rupture time and rise time for Aftershock A (left) and Aftershock B (right) as mapped onto the Northridge fault plane.

Acknowledgments

This research was funded by the National Science Foundation through Cooperative Agreement EAR-8920136 to the Southern California Earthquake Center.

References

[1] Archuleta, R. J. (1984). A faulting model for the 1979 Imperial Valley earthquake, *J. Geophys. Res.*, **89**, 4559-4585.

[2] Hartzell, S. H. and T. Heaton (1983). Inversion of strong ground motion and teleseismic waveform data for the fault rupture history of the 1979 Imperial Valley, California, earthquake, *Bull. Seismol. Soc. Am.*, **73**, 1553-1583.

[3] Wald, D. J., D. V. Helmberger, and T. H. Heaton (1991). Rupture model of the 1989 Loma Prieta earthquake from the inversion of strong-motion and broadband teleseismic data, *Bull. Seismol. Soc. Am.*, **81**, 1540-1572.

[4] Zeng, Y., K. Aki and T. Teng (1993). Mapping of the high-frequency source radiation for the Loma Prieta earthquake, California. J. *Geophys. Res.*, **98**, 11981-11993.

[5] Cocco, M. and J. Boatwright (1993). The envelopes acceleration time histories, *Bull. Seismol. Soc. Am.*, **83**, 1095-1114.

[6] Kakehi, Y. and K. Irikura (1996). Estimation of high-frequency wave radiation areas on the fault plane by the envelope inversion of acceleration seismograms. *Geophys. J. Int.*, **125**, 892-900.)

[7] Kakehi, Y. and K. Irikura (1997). High-frequency radiation process during earthquake faulting-envelope inversion of acceleration seismograms from the 1993 Hokkaido-Nansei-Oki, Japan, earthquake, *Bull. Seismol. Soc. Am.*, **87**, 904-917.

[8] Hartzell, S. H., P. Liu and C. Mendoza (1996). The 1994 Northridge, California, earthquake: Investigation of rupture velocity, rise time and high-frequency radiation, *J. Geophys. Res.*, **101**, 20091-20108.

[9] Hartzell, S. H. (1978). Earthquake aftershocks as Green's functions, *Geophysical Research Letters*, **5**, 1-4.

[10] Madariaga, R. (1977). High-frequency radiation from crack (stress drop) models of earthquake faulting, *Geophys. J. R. Astron. Soc.*, **51**, 625-651.

[11] Madariaga, R. (1983). High-frequency radiation from dynamic earthquake fault models, *Ann. Geophys.*, **1**, 17-23.

[12] Das, S. and K. Aki (1977). Fault planes with barriers: A versatile earthquake model, *J. Geophys. Res.*, **82**, 5648-5670.

[13] Liu, P., S. Hartzell and W. Stephenson (1995a). Nonlinear multiparameter inversion using a hybrid global search algorithm: Applications in reflection seismology, *Geophys. J. Int.*, **125**, 991-1000.

[14] Liu, P., C. Ji, and S. Hartzell (1995b). An improved Simulated annealing Downhill simplex hybrid global inverse algorithm, *Chinese J. Geophysics*, **38**, 377-383.

[15] Aki, K. (1967). Scaling law of seismic spectrum, J Geophys. Res., **72**, 1217-1231.

[16] Brune, J. (1970). Tectonic stress and the spectra of seismic shear waves from earthquake. *J Geophys. Res.*, **75**, 4997-5009.

[17] Sen, M. K. and P. L. Stoffa (1991). Nonlinear one-dimensional seismic waveform inversion using simulated annealing, *Geophysics*, **56**, 1624-1638.

[18] Wald, D. J., T. H. Heaton, and K. W. Hudnut (1996). The slip history of the 1994 Northridge, California, earthquake determined from strong-motion, teleseismic, GPS, and leveling data, *Bull. Seismol. Soc. Am.*, **86**, S49-S70.